HIGH-RESOLUTION PHOTOACOUSTIC TOMOGRAPHY *IN VIVO*

Lihong V. Wang[1], Meng-Lin Li[1], Hao F. Zhang[1], Konstantin Maslov[1], and George Stoica[2]

1. Optical Imaging Laboratory, Department of Biomedical Engineering, Texas A&M University
2. Department of Veterinary Pathobiology, Texas A&M University

Corresponding author: Email: lwang@tamu.edu; URL: oilab.tamu.edu; TEL: 979-847-9040; FAX: 979-845-4450

ABSTRACT

An *in vivo* backward-mode photoacoustic microscope was recently developed that employs a high frequency, broadband, large numerical aperture (NA) focused ultrasonic transducer to provide high resolution and high sensitivity. However, out of the focus region, the limited depth of focus deteriorated the image quality significantly. Based on a virtual-detector concept, we devised and implemented a synthetic aperture focusing technique in combination with coherence weighting to overcome this drawback. This technique improved the –6-dB lateral resolution from 50–265 microns to 46–55 microns and increased the SNR by up to 23 dB. *In vivo* experiments showed that the technique provided a clearer representation of the vascular distribution in the dorsal dermis of a rat.

1. INTRODUCTION

Photoacoustic imaging combines the merits of both optics and ultrasound and, therefore, provides high optical contrast and high acoustic resolution, and can be applied to measuring the optical properties of biological tissues noninvasively. It is a promising technique for vasculature structural imaging [1]-[3], epidermal melanin measurement [4][5], breast tumor detection [5], and oxygenation monitoring in blood vessels [7]. Recently, an *in vivo* backward-mode confocal photoacoustic microscope (PAM) with dark-field illumination was developed by Maslov et al. to image blood vessels in the skin [8]. This system is capable of imaging optical absorption contrasts as deeply as 3 mm in biological tissue with high lateral resolution (45 μm at the focal point) and high axial resolution (~15 μm). This PAM system shows potential for applications in dermatology and related cancer research. To achieve high image resolution and high sensitivity, a high-frequency, wide-band, large numerical-aperture (NA) spherically focused ultrasonic transducer, which is coaxial and confocal with the optical illumination, is employed in this system. The tradeoff in using such a large NA ultrasonic lens, however, is the limited depth of focus, which deteriorates the image quality significantly in the out-of-focus region. Here, we investigate a virtual point-detector based synthetic aperture focusing technique (SAFT), combined with coherence weighting, to extend the depth of focus for a PAM with this type of large-NA transducer.

2. VIRTUAL-DETECTOR BASED SAFT

In virtual-detector based SAFT, the focal point of the transducer is viewed as a virtual point detector, as illustrated in Figure 1(a). When biological tissues absorb pulsed laser energy, photoacoustic (PA) waves generated within a certain solid angle are assumed to be detected by the virtual detector. If a linear scan is performed, the PA radiation pattern from the virtual detector at that current position will overlap with the PA radiation pattern produced at adjacent positions. Hence, synthetic aperture focusing can be performed in the overlapped region above and below the virtual detectors. For example, the two black spots in the overlapped region before and after the virtual detectors can be synthetically focused using the received scan lines when both of the two points are in the PA radiation patterns.

Figure 1(b) shows the focusing geometry of SAFT with virtual detectors. The PA radiation pattern of the scan line *i,* with a distance x_i away from the synthesized beam axis, covers the desired synthetic focal point *p*. Hence, the PA signals from scan line *i* can be added to the synthesized beam constructively by applying an appropriate time delay. Based on the virtual detector concept, the acoustic propagation time (i.e., the received time delay), from the synthetic focal point *p* to the virtual detector f_i at scan line *i*, can be expressed as:

$$\Delta t_i = \mathrm{sgn}(z - z_f) \cdot \frac{r'}{c}, \tag{1}$$

where z_f is the transducer's focal length; z is the depth of the synthetic focal point *p* from the transducer surface; r' is the distance from the virtual detector to the synthetic focal point; c is the acoustic velocity; and sgn(·) is the signum function. Note that a negative time delay is applied if the synthetic

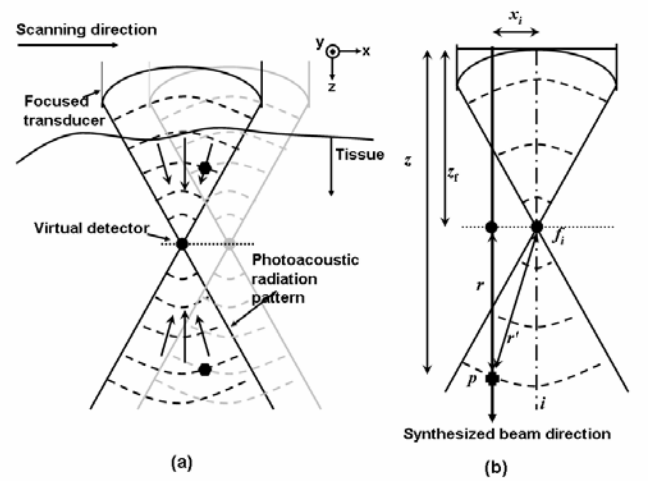

Figure 1. (a) Schematic of the virtual detector concept. (b) Focusing geometry of SAFT with a virtual detector.

focal point is shallower than the focal point of the transducer.

The virtual-detector based SAFT is accomplished by applying appropriate delays relative to the virtual point detector to the adjacent scan lines according to (1) and then summing the delayed signals [9]:

$$S_{\mathrm{SAFT}}(t) = \sum_{i=0}^{N-1} S(i, t - \Delta t_i) \ , \qquad (2)$$

where $S(i,t)$ is the received signal at scan line i, and N is the maximum number of scan lines included in the sum. N is determined by the angular extent of the PA radiation pattern, which is primarily related to the parameters of the ultrasonic transducer since the light distribution is much broader due to the strong light scattering in biological tissue. In addition to improving the lateral resolution in the out-of-focus region, SAFT can increase the SNR as well.

3. CF WEIGHTING

In addition to virtual-detector SAFT, a coherence factor (CF) of the delayed signals at each SAFT imaging point can be used as a weighting factor to further improve the focusing quality. CF is defined as [10]:

$$\mathrm{CF}(t) = \frac{\left| \sum_{i=0}^{N-1} S(i, t - \Delta t_i) \right|^2}{N \cdot \sum_{i=0}^{N-1} \left| S(i, t - \Delta t_i) \right|^2} , \qquad (3)$$

which is a real quantity ranging from 0 to 1 that indicates the degree of in-phase addition among the delayed signals. Figure 2 illustrates the idea of CF weighting. In Figure 2, the vertical axis is the depth, and the horizontal axis denotes the lateral position. The left panel shows the simulated point spread function (PSF) after SAFT. The middle panel is its corresponding CF map. The definition of CF implies that because of the constructive summation of the delayed signals (i.e., highly in phase), the CF at the main lobe of the PSF is

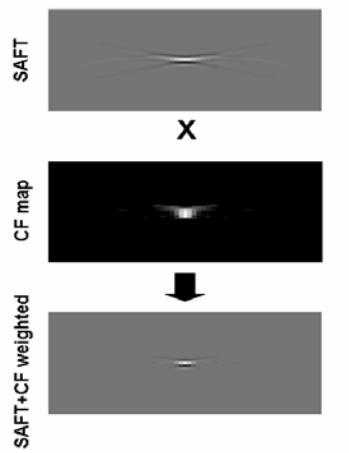

Figure 2. Illustration of CF weighting

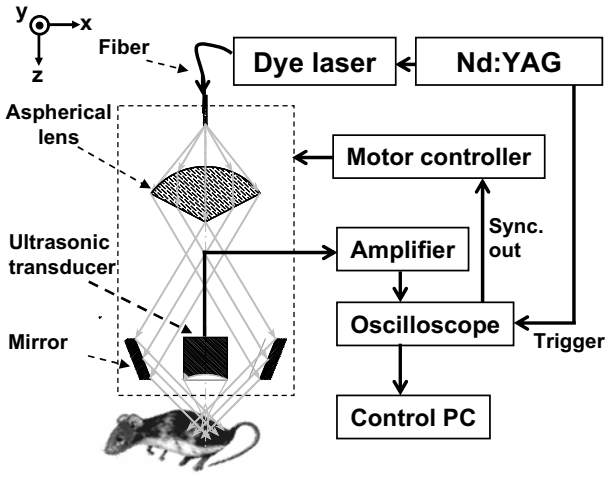

Figure 3. Schematic diagram of experimental setup

high (close to 1), whereas the CFs at the side lobes are low due to destructive summation. Based on this property, after being multiplied by the corresponding CF map on a point-by-point basis, the side lobes in SAFT are suppressed; thus the synthesized beam quality is improved, as shown in the right panel. CF weighting can also reduce the elevated side lobes in SAFT that result from sound velocity inhomogeneity in the tissue [11]. Moreover, it can suppress background noise because the measurement noise is generally out-of-phase.

4. EXPERIMENTAL RESULTS

The *in vivo* dark-field backward-mode PAM developed by Maslov et al. was used in this study. A schematic diagram of the experimental setup is shown in Figure 3. A tunable dye laser (ND6000, Continuum), pumped by an Nd:YAG laser (Brilliant B, Bigsky), was employed to provide laser pulses with a FWHM of 6.5 ns, a wavelength of 584 nm, and a pulse repetition rate of 10 Hz. The laser energy was delivered by a 0.6-mm diameter optical fiber whose output

was coaxially positioned on a three-dimensional precision translation stage driving an ultrasonic transducer with a 50-MHz center frequency and a 70% nominal bandwidth (V214-BC-RM, Panametrics). An in-house-constructed acoustic lens provided an NA of 0.44 and a focal length of 6.7 mm. The PA signals were amplified by a broadband amplifier (ZFL-500N, Mini-Circuits) and then were acquired at a 250 MHz sampling rate by a digital oscilloscope (TDS 5034B, Tektronics), triggered by the Nd:YAG laser and used to synchronize the motor controller. The incident energy density on the sample surface was controlled to <1 mJ/cm^2. In SAFT, each scan line was first interpolated by a factor of eight to increase the delay accuracy, and the acoustic velocity was assumed to be 1.5 mm/μs. Note that the PA images shown here were taken without signal averaging to minimize the data acquisition time.

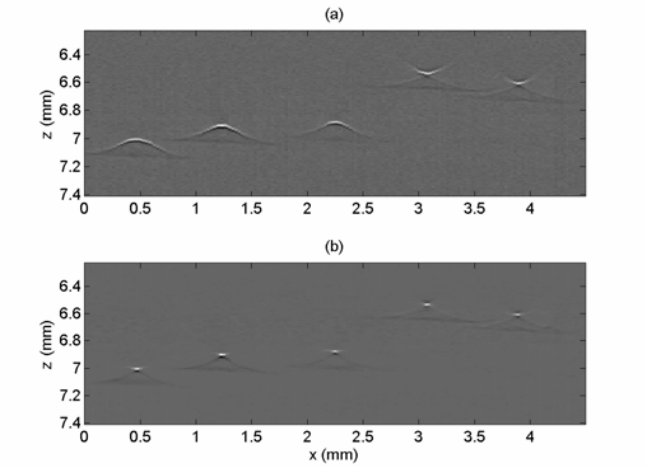

Figure 4. B-scan images of an Intralipid phantom containing five embedded 6-μm carbon fiber, which was scanned at various depths. (a) Original image (b) SAFT + CF weighted image.

4.1 Phantom of carbon fiber

The PSF of the PAM was evaluated using a cross-sectional view of a carbon-fiber phantom. This phantom was composed of five 6-μm carbon fibers immersed at different depths in a diluted Intralipid solution (Clintec Nutrition Company, Dearfield, Illinois). The scanning step size was 25 μm. Note that the maximum number of scan lines for the beam synthesis was limited, in this case, to 20. This limitation reduced the implementation complexity of SAFT. Figure 4 shows (a) the original B-scan image and (b) the SAFT + CF weighted image. The two images are shown on the same linear gray scale. The brightness represents the laser-induced photoacoustic pressure detected by the transducer. The vertical axis is the depth from the transducer surface, and the horizontal axis is the lateral position. In Figure 4(a), due to the limited depth of focus of the transducer, the farther the carbon fiber is away from the focal point, the wider the lateral extent, which indicates poorer lateral resolution. The SAFT + CF weighted image exhibits improved lateral resolution.

The –6-dB lateral and axial resolutions as well as the improved SNR at all of the imaging depths are estimated. The SAFT+CF weighting provides depth independent lateral resolution, reducing the –6-dB width of the imaged carbon fiber from 50–265 μm to 46–55 μm, depending on the distance from the ultrasonic focal point, without affecting the axial resolution (the estimated –6-dB axial resolution is about 11 μm). In addition, the SAFT + CF weighting improves the SNR by up to 23 dB. Here, the SNR is defined as the ratio of the maximal intensity at the carbon fiber position to the average noise intensity.

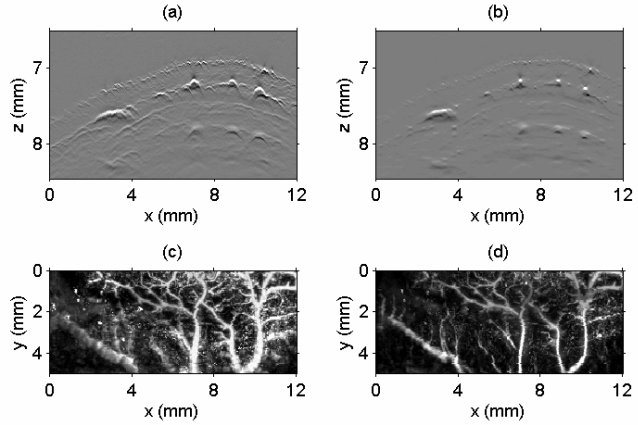

Figure 5. (a) and (b) *In vivo* B-scan images (c) and (d) *In vivo* projected C-scan images of the rat's dorsal dermis; (a) and (c): Original; (b) and (d): SAFT + CF weighted.

4.2 *In vivo* imaging of rats

In vivo experiments on rats were also conducted to further evaluate the efficacy of the proposed technique. The dorsal dermis of Sprague Dawley rats (~150 g, Charles River Breeding Laboratories) was imaged. Before imaging, the hair on the backs of the rats was removed using commercial hair remover lotion. Anesthesia was administrated by intramuscular injection of ketamine hydrochloride (44 mg/kg), xylazine hydrochloride (2.5 mg/kg), acepromazine maleate (0.75 mg/kg), and atropine (0.025 mg/kg). After the experiments, the rats recovered normally without any noticeable health problems. The laboratory animal protocol for this work was approved by the University Laboratory Animal Care Committee of Texas A&M University.

Figures 5(a) and (b) show the *in vivo* original and the SAFT+CF weighted B-scan images of a rat's dorsal dermis. To enlarge the imaging area and reduce the scanning time, we used a step size of 50 μm. The maximum number of scan lines for beam synthesis was limited to 10 to reduce motion artifacts. The two images are displayed in the same linear gray scale. The vertical axis is the depth, and

the horizontal is the lateral scanning position. Figure 5(b) exhibits better definition of the vessel positions than the original image 5(a) over the entire depth of imaging field. Figure 5(c) (original) and (d) (SAFT+CF weighted) are *in vivo* projected C-scan images of a rat's dorsal dermis showing the vascular network, in which the maximum of each scan line along the depth direction versus the 2D transducer position is plotted. Figure 5(d) provides a clearer vascular distribution than Figure 5(c) as a result of the improved lateral resolution and SNR, as shown in Figure 5(b). Note that here SAFT + CF weighting was performed for each B-scan along the *x* direction; hence only the lateral resolution in the *x* direction is improved.

5. CONCLUDING REMARKS

In this paper, we investigated a virtual-detector based synthetic aperture focusing combined with coherence weighting, to extend the depth of focus for photoacoustic microscopy with a large-NA transducer. The virtual-detector focusing technique significantly improves the degraded lateral resolution in the out-of-focus region of the PAM system when employing a large NA ultrasonic transducer. The CF weighting employed here can also reduce the elevated side lobes in SAFT caused by phase and amplitude distortions of acoustic signals resulting from sound velocity inhomogeneity in the tissue. In [11], it was shown that the CF weighting can improve degraded beam quality for one-way distortion up to one quarter wavelength on reception. The phantom and *in vivo* experimental results demonstrate the efficacy of this technique: depth independent lateral resolution is achieved, and the SNR is also improved. The extended depth of focus for the PAM system enables 3D reconstruction of the vascular network for the study of tumor angiogenesis. In addition, 2D SAFT can be used to obtain even better image quality if a higher pulse-rate laser is used to increase the scanning speed and thus reduce motion artifacts.

6. REFERENCES

[1] X. Wang, Y. Pang, G. Ku, X. Xie, G. Stoica, and L. V. Wang, "Noninvasive laser-induced photoacoustic tomography for structural and functional in vivo imaging of the brain," *Nat. Biotechnol.* 21, pp. 803–806, 2003.

[2] G. Ku, X. Wang, X. Xie, G. Stoica, and L. V. Wang, "Imaging of tumor angiogenesis in rat rains in vivo by photoacoustic tomography," *Appl. Opt.* 41, pp. 770–775 ,2005.

[3] J. J. Niederhauser, M. Jaeger, R. Lemor, P. Weber, and M. Frenz, "Combined ultrasound and optoacoustic system for real-time high-contrast vascular imaging in vivo," *IEEE Trans. Med. Imag.* 24, pp. 436–440 , 2005.

[4] E. V. Savateeva, A. A. Karabutov, B. Bell, R. Johnigan, M. Motamedi, and A. A. Oraevsky, "Non-invasive detection and staging of oral cancer in vivo with confocal optoacoustic tomography," *Proc. SPIE* 3597, pp. 55–66 , 2000.

[5] J. A. Viator, L. O. Svaasand, G. Aguilar, B. Choi, and J. S. Nelson, "Photoacoustic measurement of epidermal melanin," *Proc. SPIE* 4960, pp. 14–20, 2003.

[6] R. O. Esenaliev, A. A. Karabutov, and A. A. Oraevsky, "Sensitivity of laser opto-acoustic imaging in detection of small deeply embedded tumors," *IEEE J. Sel. Top. Quantum Electron.* 5, pp. 981– 988, 1999.

[7] R. O. Esenaliev, I. V. Larina, K. V. Larin, D. J. Deyo, M. Motamedi, and D. S. Prough, "Optoacoustic technique for noninvasive monitoring of blood oxygenation: a feasibility study," *Appl. Opt.* 41, pp. 4722–4731, 2002.

[8] K. Maslov, G. Stoica, and L. V. Wang, "In vivo dark-field reflection-mode photoacoustic microscopy," *Opt. Lett.* 30, pp. 625–627, 2005.

[9] M.-L. Li, W. J. Guan, and P.-C. Li, "Improved synthetic aperture focusing technique with application in high-frequency ultrasound imaging," *IEEE Trans. Ultrason., Ferroelect., Freq. Contr.* 51, pp. 63– 70, 2004.

[10] C.-K. Liao, M.-L. Li, and P.-C. Li, "Optoacoustic imaging with synthetic aperture focusing and coherence weighting," *Opt. Lett.* 29, pp. 2506–2508, 2004.

[11] P.-C. Li and M.-L. Li, "Adaptive imaging using the generalized coherence factor," *IEEE Trans. Ultrason., Ferroelect., Freq. Contr.* 50, pp. 128–141, 2003.